Khadija EL KAMOUNY[1],*,
Hassane MAHMOUDI[2],
Brahim LAKSSIR[1]

Solar Charger Sizing

As a part of the optimization of photovoltaic energy extraction, an optimization of each individual component is required. This paper focuses on the optimization of solar battery charger block and presents a new method to track the maximum power point and the load regulation. For this purpose, we proposed a specific architecture and design of a high-reliable, robust, stable, miniaturized system. We sized a photovoltaic charger to regulate the battery charger that employs an intelligent algorithm including the criteria of reliability.

1. Introduction

Batteries are devices for storing electrical energy in a chemical form. They are widely used in portable devices, emergency power supplies, Solar Fields. To benefit continuously from the renewable energy specially the solar one, for some isolated communities, a means of energy storage is required. The more useful way is charging batteries. The charging of the batteries is performed by an electronic system that has a considerable impact on the battery life. In this paper, a particular attention is paid to the conception of an electronic charger. We will detail the steps of the design process of a battery charger using a solar panel 250W.

2. Modeling

As a result of the analysis of different system of solar energy conversion, the architecture drawn in Figure 1 is proposed. In this figure, the first block converts the input DC voltage to a high frequency AC voltage by a high frequency transformer. The transformer output maintains a voltage of 311 V as a maximum value to get a RMS voltage of 220 V at the end of the circuit. This voltage is rectified before being corrugated again at a frequency of 50 Hz. A second unit is added to charge the battery by a voltage of 12 V. In this article, we will focus on the sizing of the second block (battery charger).

2.1. Theoretical Aspects

2.2. Battery Types

A battery is characterized by a battery voltage in volt (V), a battery capacity C in Ampere-hour (Ah), and a maximum current, which is important in the case of engine start. Depending on the technology, there are four major types of batteries: Lead (Pb), Nickel Cadmium (Ni-Cd), Nickel Metal Hydride (NiMH) and lithium (Li) batteries.

---

* Corresponding author: K. EL KAMOUNY, Electrical Department, Mohammed V-Agdal University Ecole Mohammadia d'Ingénieurs « EMI » Rabat, Morocco, E-mail: k.elkamouny@mascir.com
[1] Moroccan foundation for Advanced Science, Innovation and Research « MAScIR » Rabat Design Center, Avenue Mohamed El Jazouli - Madinat Al Irfane 10100 Rabat – Morocco.
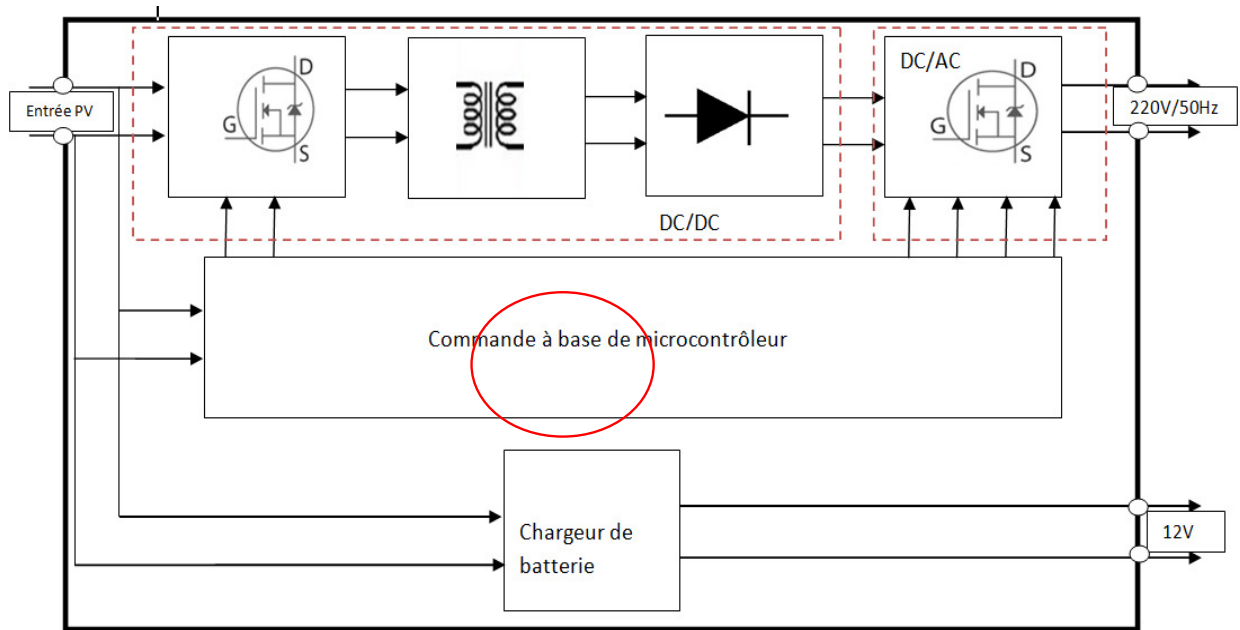[2] Electrical Department, Mohammed V-Agdal University Ecole Mohammadia d'Ingénieurs « EMI » Rabat, Morocco

Fig.1. Block diagram of the solar energy conversion system

Table 1: Four major types of batteries

Specifications	Lead (Pb)	Nickel-Cadmium (Ni-cd)	Nickel Métal Hydride (Nimh)	Lithium (Li):Li-ion et Lipo
Energy / weight	20 - 40Wh/kg	20 -40Wh/kg	30 - 80Wh/kg	100 - 250Wh/kg
Energy/volume	40 - 100Wh/l	50 - 150Wh/l	140 - 300Wh/l	200 - 620Wh/l
Life duration	4 - 5 years	2 - 3 years	2 - 4 years	7 years
number of charge cycles	400 - 1200 cycles	1500 cycles	500 - 1200 cycles	1200 cycles
Voltage / item	2.1V	1.2V	1.2V	3.6V or 3.7V

A comparative study is made between the different types of batteries available in the market today and the lead technology batteries is chosen to be used for this application, because this type of batteries represent nearly 65 % of the battery market and are widely used in the automotive, traction, photovoltaic, power supplies appliances. Further, the technology of lead-acid batteries is considered.

2.3. Algorithm of the Charging

The charging of a battery follows several laws. A battery charges by applying DC for a limited time. This charge occurs in three phases. The first phase is a constant current charge, when a constant current is applied to the battery and the voltage increases up to a value V_{gaz} called voltage gasification electrolyte (2.35 V/cell). The second phase is a constant voltage charge or an absorption phase, when the battery voltage is set at 2.35 V/cell to continue the charge, and the current decreases to a minimum value. In the

118

third phase, the battery can be left in a maintaining regime or be disconnected. The maintaining regime is characterized by sustaining the nominal voltage with a current, which is generally equal to the 0.001^{th} of the battery capacity. These phases are illustrated in Figure 2 taken from [1].
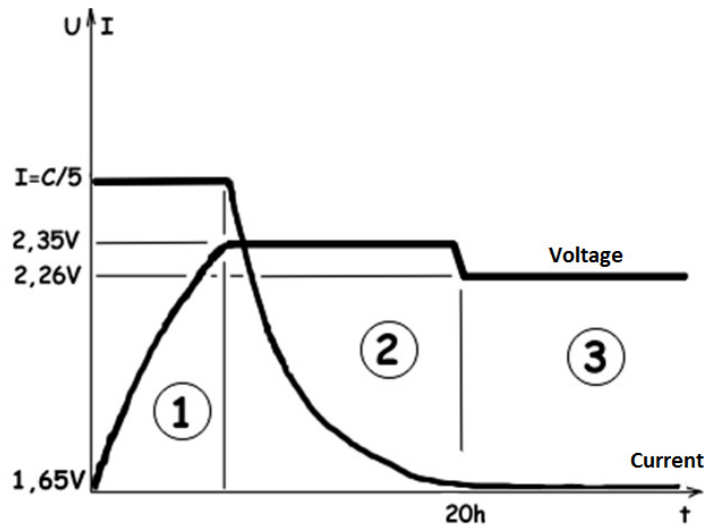

Fig.2: Charging cycle of a Lead Acid Battery.

Battery charger is usually packaged around the converter as well as a rectifier and especially a chopper for solar chargers. Then, consider the implementation of, the well-known one, Buck converter in a battery charger.

Buck Converter

Choppers are DC converters. There are several types of converters according to the ratio between input and output variables.
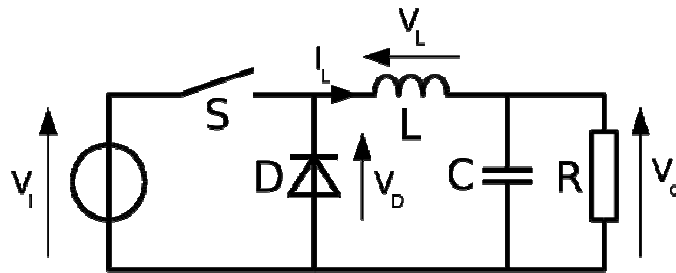
2.4. **Theoretical Schematic**

Fig.3: Buck Converter Schematic

The chopper is composed of a switch S, which controls the flow of energy from the source to a load R. A free-wheeling diode allows the discharge of the inductor L to the load R. The capacitor C is used to filter the output voltage. The schematic operates in the two phases. The first phase is occurring during the time t, where $0 < t < \alpha T$, T is the period of an input electrical signal, α is the duty cycle. The switch S is ON and the diode is OFF. The coil L is charged through the generator V_i. During the second phase by $\alpha T < t < T$, the energy stored in the coil is discharged into the load R through the diode D. This regime is called freewheeling operation. The average value of the output voltage is $V_0 = \alpha V_i$. The duty cycle α is the ratio between the pulse duration of the signal in the high state and its period T. The α varies between 0 and 1, so the output voltage V_0 also changes between 0 and V_i.

The control signal is generated by circuits as NE555, microcontrollers, etc. Also some specific circuits for the control of choppers are used. One of them is LT3845A from Linear Technology [2]. Consider the implementation of LT3845A circuit to control the buck converter. This solution allows us to develop a very robust and stable system.

LT3845A Circuit

LT3845A is an integrated circuit from Linear Technology. This circuit is dedicated to control the buck converter. It allows the control of the input and output voltage of the system. The circuitry around is shown in figure 10 is used to set the desired characteristics.
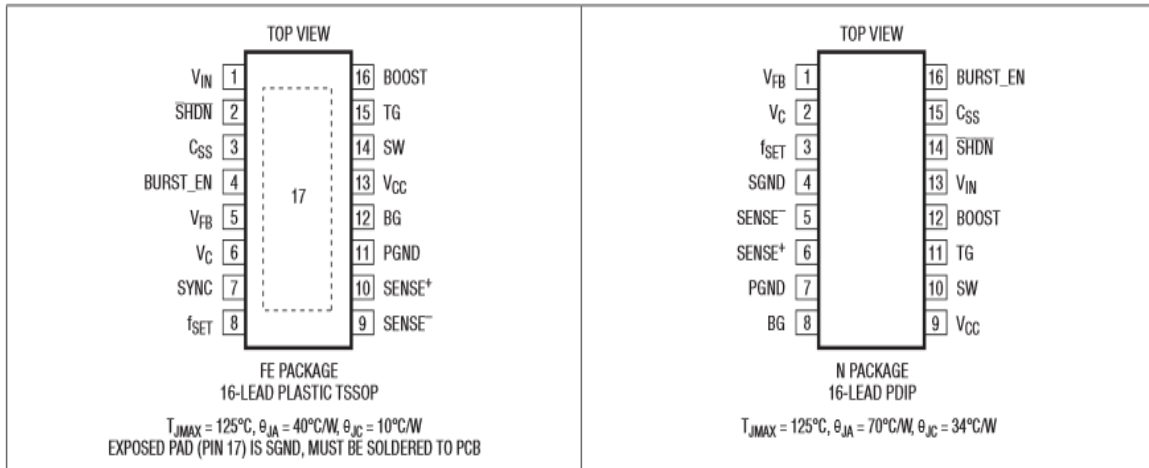

Fig. 2. LT3845A Package

Table 2: pins configuration of LT3845a [2].

N°	DESIGN	Signification.
1	Vin	Input voltage
2	$\overline{SHDN}$	Shut down the circuit.
3	C_{ss}	Soft start (slew rate)=2µA($t_{ss} / 1.231V$)
4	$Burst\_EN$	Burst mode
5	V_{FB}	Output voltage feedback
6	V_C	The voltage corresponding to the maximum current / period
7	SYNC	external clock
8	F_{Set}	Adjusting the operating frequency
9	$Sense-$	Negative current sensor
10	$Sense+$	Positive current sensor
11	BG	gate of the transistor Q2
12	V_{CC}	Internal voltage of the circuit
13	TG	Upper transistor gate
14	BOOST	The supply for the Bootstrapped

2.5. Working Principle

The circuit recovers the output voltage from the buck converter through the pin V_{FB} (voltage Feedback). The difference between this voltage and the LT3845A internal value of 1.236 V is amplified to generate a comparison signal to the threshold pin V_C for current sensors. The oscillation frequency is programmed through a resistance in the pin F_{Set} as shown in figure 10. At the beginning of a clock cycle, the control signal reaches level "1", and while the V_{FB} value reaches the value V_C the signal level falls to zero. The time to drop to the level "0" is divided by the total period that gives the duty cycle. If the threshold is not reached during the entire period, the signal is set to zero during 350 ns.

Circuit Components Selection

In this application, we will control the Buck converter by the LT3845A circuit. So, we will size the Buck converter first.

2.6. Inductor Sizing

The inductor is sized according to the rate of current ripple that flows through its turns. The following formula gives the inductance:

$$L \geq V_{out} \frac{V_{in-\max} - V_{out}}{f_{sw} V_{in-\max} \Delta I_l}$$. a ripple rate of 10% is fixed (about 40% usually).

So the theoretical inductor value is limited $L \geq 57.16 \mu H$

2.6.1. Magnetic Circuit of the Inductor

To determine the self-size of the inductor, the magnetic circuit, the cross section of copper S and the number of windings n are required.

The variables required in this calculation are the magnetic induction B in Tesla (T), the intensity of the magnetic field H in A/m, the magnetic flux Φ in weber (wb), the permeability of the material μ, $\mu_0 = 4\pi 10^{-7}$ in vacuum, relative permeability μ_e to selected material, the section of the magnetic core A_e, the effective length L_e of a line of field, and the number of turns n.

Generally, manufacturers of the magnetic circuit give the permeance A_L as: $L = n^2 A_L$

avec $A_L = \dfrac{\mu_0 \mu_e A_e}{L_e}$ [3].

But we must to check if the material is not saturated and the number of turns n can be winded on the core. The following equations will be used to determine these parameters:

2.6.2. Section of Magnetic Circuit

For the magnetic core, the MS-250 125-2 is taken from Arnol MICROMETAL. 125µH is the inductor value with n²=1000. Hence, a coil of 35 turns gives an inductor value of 150µH. However, as a constraint, the core surface must support all turns.

2.6.3. Section of Copper Wire S_c

The current density is defined δ ($\delta = 5.10^6 A/\text{m}^2$ for the copper) as the amount of charge passing through a unit of area per unit of time, that means the intensity of current per m². So, $S_c = \dfrac{I_{max}}{\delta}$, $S_c = 5.2mm^2$ minimum with a current value 26 A (in this case we can put a several lower section wires in parallel).

2.7. Input Capacity

This capacity reduces the fluctuations of the input voltage as shown in figure 10.

$$C = \frac{I_{out-max}V_{out}}{f_{sw}V_{in-min}\Delta V_{in}} = 9.34\mu F$$

2.8. Schottky diode

The diode is replaced by a MOSFET to benefit from a lower threshold voltage (0.5V). It was selected according to the drain / source voltage, the drain current and the operating frequency. The IRFP4321 were chosen for this application.

2.9. Output Voltage Regulation

A voltage divider circuit is connected to the pin "FB". These circuit parameters are calculated as follows: $R_2 = (\dfrac{V_{out}}{1.231} - 1)R_1$. [5] with $R_1 = 10K\Omega$, then $R_2 = 103K\Omega$.

2.10. Rise Time of the Charge Voltage

The rise of the output voltage is set by the C$_{ss}$ capacity value $C_{ss} = \dfrac{2\mu A.t_{ss}}{1.231V}$. [5]

2.11. Programming the Operating Frequency

A resistor connected to the pin F_{Set} is used to set the frequency. The values of the resistor depending on the frequency are reported in the following table.

Table 3: the resistor R_{set} $(K\,\Omega)$ depending on the operating frequency [4]

R$_{SET}$ (kΩ)	f$_{SW}$ (kHz)
191	100
118	150
80.6	200
63.4	250
49.9	300
40.2	350
33.2	400
27.4	450
23.2	500

2.12. Resistor Current Sensor

A resistor is used as current sensor. Its value is calculated as:

$$R_{sense} = \frac{100mV - 45mV(\frac{V_{out}}{V_{in}})}{I_{max}} = 2m\Omega$$

, [5] a resistor of $5m\Omega / 10W$ is taken.

2.13. LTC4000-1 Circuit

The LTC4000-1 is an integrated circuit from LINEAR TECHNOLOGY [5], and is used to control the charge process of the batteries. It includes a MPPC controller (Maximum Power Point Controller) when the charger input is a photovoltaic panel.

Table 4: Pins configuration of LTC4000-1 [5]

N°	DESIGN	Signification
1	ENC	To start the charge of the batteries
2	IBMON	Charge current of the battery
3	CX	Current of the end of charging cycle
4	CL	Limited Current of charge
5	TMR	Charge duration
6	GND	Ground
7	FLT	indicator of temperature overflow or battery fault
8	CHRG	State of charge.
9	BIAS	Output of a 2.9V regulator
10	NTC	Resistor with a negative temperature coefficient to control the battery temperature.
11	FBG	Feedback ground pin. This pin is connected to the ground through 100Ω while Vin>3V, otherwise it is disconnected to prevent the two divider bridge to drain the current from the battery.
12	BFB	Battery feedback voltage. Is used to set the voltage of the charge.
13	BAT	Connection to the battery.
14	BGATE	The gate of a PMOS which allows the battery to provide power to a load.
15	CSN	Connecting the battery current sensor (negative side).
16	CSP	Connecting the battery current sensor (positive side).
17	OFB	Output voltage feedback

| 18 | IGATE | Gate of a PMOS (ideal diode) which cuts the input if it is not valid (3-60V). |
19	IID	Input Ideal Diode
20	IHT	High impedance control. Indicates the achievement of regulation loops thresholds. Once achieved its threshold, it reduces the current to 1mA.
21	CC	Converter compensation pin
22	CLN	Input current sense negative.
23	IN	Input voltage
24	GND	Ground
25	VM	Voltage monitoring, input voltage control (RST)
26	RST	If VM < 1.193, RST= 0.
27	IIMON	Input current monitoring
28	IFB	Input voltage monitoring. If IFB < 1, IHT goes to 0 to reduce the input charge.
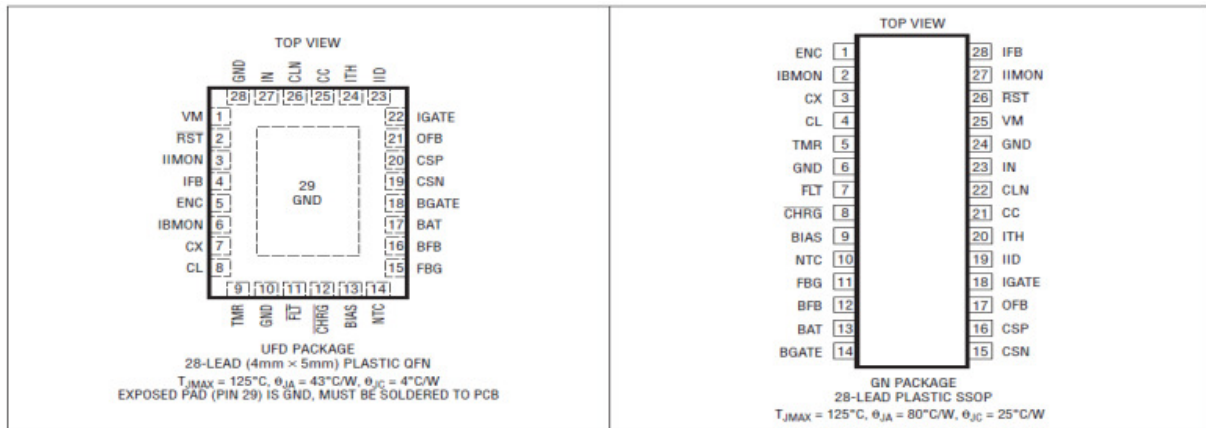
Fig.5: Package of LTC4000-1.

2.13.1. Working Principle

The LTC4000-1 [3] is designed for battery charging applications with high input voltage. It includes four control loops: the control loop of the input voltage, of the current and the charging voltage, of the battery, and finally the loop of the output voltage. The input regulation ensures that the input voltage is not less than the programmed level. The control loop of the charge current ensures that the current value does not exceed the pre-set value (programmed value). The loop of charge voltage (value indicating that the battery is charged) and the output voltage, also, ensure that the programmed values are not exceeded.

2.13.2. Circuit Features.

2.13.2.1. Input Voltage Regulation

In the most of DC power supplies, the output voltage drops when the current required increases. So, there is a voltage at which the output power is maximum (case of PV generators). It is then possible to program this voltage on LTC4000-1, so the voltage will not get lower.

Charge Regulation

The circuit regulates the current, the charging voltage of the battery and the output voltage of the system. The system tests first, if the battery is deeply discharged ($V_{BFB} < V_{LOBAT}$). Whether a slow charging process (0.1^{th} of the load current) is achieved and a timer is started. At the end of the programmed time, the condition ($V_{BFB} < V_{LOBAT}$) is tested again in order to conclude that the battery is defective and the charging process is stopped. Otherwise, the normal charging process is started. The end of charging process can be programmed in two ways:

- If TMR is connected to BIAS, charging process is stopped when the minimum value is reached.
- If capacity is connected to the TMR pin, the charging process is delayed. This timer is started with the beginning of the constant voltage charging phase. The process stops as soon as the timer is expired.

At the end of the charging process, if the input source is not able to provide the required current to the load, the battery may contribute to provide this current. At a discharge level of 97.1%, a new charge cycle is initiated.

2.13.3. Components Sizing
2.13.3.1. PMOSFET at the Input

The input IC is a PMOS transistor which mainly supports the input power and has a very low resistor value R_{dson}, is used as an ideal diode. It is chosen from VISHAY series Si7135DP. [3] ($60A$, $R_{dson} = 0.004\Omega$, $V_{gsmax} = -30V$).

$$R_{cs} = \frac{V_{CL}}{20.I_{CLIM}} \text{ So } R_{CL} = \frac{V_{CS}I_{CLIM}}{2.5\mu A} = 40K\Omega \text{ [5]}$$

R_{CL} allows the setting of the limit of the charging current.

Selection of Charging Voltage

The output voltage is set by a divider bridge. Thus, the resistor value is calculated as follows [5]:

$$R_1 = (\frac{V_{float}}{1.136} - 1)R_2 \text{ with } R_2 = 100K\Omega, \text{ then } R_1 = 1088K\Omega$$

Output Voltage

It is set using a voltage divider bridge. Consider $R_2 = 100K\Omega$, then $R_1 = 1073K\Omega$.

Threshold Voltage Switching

$$R_{VM1} = (\frac{V_{VM}}{1.193} - 1)R_{VM2} \text{ ; [3] with } R_{VM2} = 10k\Omega, \text{ then } R_{VM1} = 216K\Omega.$$

Voltage MPP

$$R_{IFB1} = (\frac{V_{VM}}{1V} - 1)R_{IFB2} \ ; [3] \text{ with } R_{IFB2} = 10K\Omega, \text{ then } R_{IFB1} = 290K\Omega.$$

2.14. Selection of heat sinks

The electronic power components, crossed by strong currents, are the seat of heat dissipation. This heating can destroy them if it is not quickly evacuated. It is therefore important to properly size heat sinks to prevent the destruction of these components. This choice is often confronted with the space board constraint. Preliminary calculations are needed to avoid unnecessary oversized radiators.

2.14.1. Dissipated Power in the Components

The first step consists of the calculation of the dissipated power that must be evacuated by the heat sink. This loss has two origins, namely losses during conduction and switching losses in the (ON / OFF and OFF / ON).

In this system, the power losses will be calculated for the two transistors (IRFP4321, TO-247AC box):

P_{cond} : Losses during conduction;

P_{com} : Losses during switching;

P_t : Losses into the transistor.

$$P_t = P_{cond} + P_{com}$$
$$P_{cond} = R_{on}I^2 = 1.2W$$
$$P_{com} = 2V_{in}^2 I_{out-\max} f_{sw} C_{RSS} = 0.22W$$

Total losses in the transistor are $P_t = 1.42W$.

2.14.2. Calculation of Thermal Resistor value heater-Air R_{thra} .

The heat dissipating chain of the cell of the switching operation (MOSFET and the diode) is:
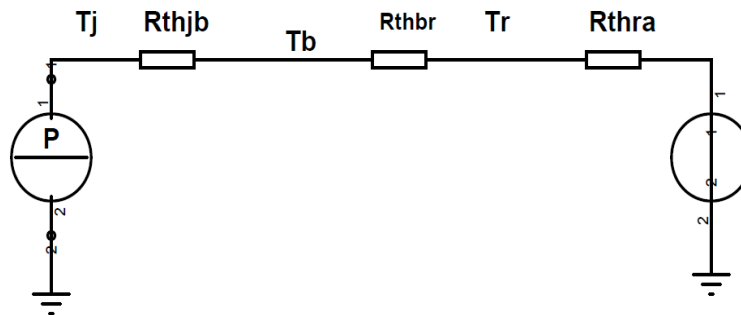

Fig.**6**: chain of thermal transfer of power components

-     R_{thjb} is the thermal resistor of junction-package;

-     R_{thra} is the thermal resistor air heater;

- R_{thbr} is the resistor case-radiator ;

- T_j is the junction temperature;

- T_b is the temperature of the housing;

- T_a is the ambient temperature is about 50 ° C (for more safety).

In this chain, it remains to determine R_{thra} .

$$R_{thra} = \frac{(T_j - T_a - P_d(R_{thjb} + R_{thbr}))}{P_d} = 5.45°C/W .$$

The sink whose thermal resistor is less than those found above is then chosen for the both types of component transistors and diodes.
We could even from this chain, calculate the junction temperature for a given ambient temperature by the following expression $T_j = T_a + P_d(R_{thjb} + R_{thbr} + R_{thjb})$. Consider the example where $T_a = 30°C$; it would be $60°C$ in the junction of the diode and $74.4°C$ in the junction transistor.

3. Simulation and Results

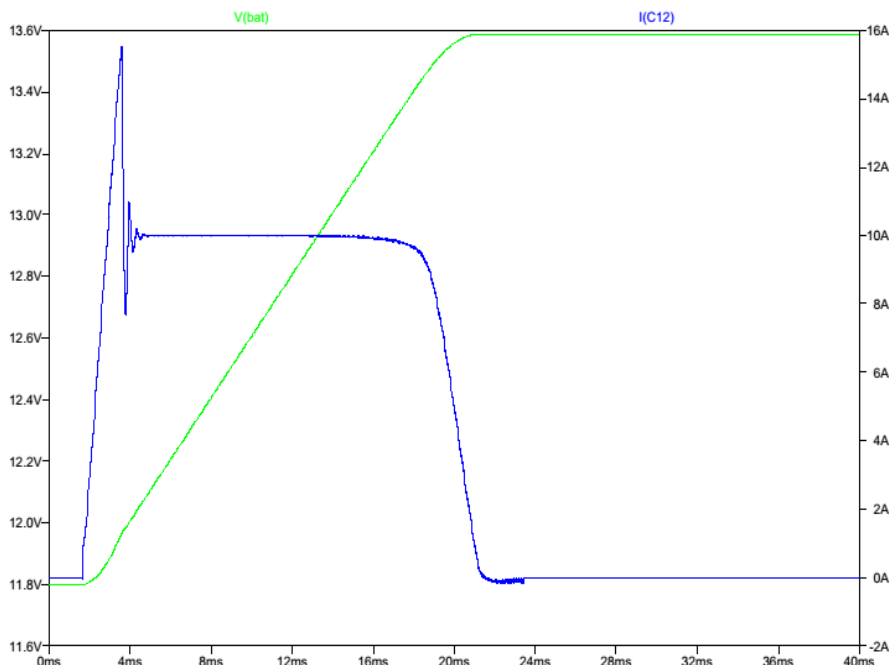The simulation results are shown in the figure *7*.

Fig. 7: charging a lead battery (simulation result on LTSpice)

The blue curve: charge current of the battery (A).

The green curve: charge voltage of the battery (V).

In this graph, there is a phase transition that takes a few milliseconds followed by a phase of constant current charge which lasts about 15ms .- depends on the capacity of the battery

to be charged - and finally charging phase at constant voltage and decreasing current. For this simulation, a model of lead acid battery of low capacity is chosen to fastly see the charging algorithm.

An auto-reversing system is foreseen to allow the battery to supply a load at the output. Automatically, a new charging cycle is started when the battery is discharged at 97.1% of its capacity.
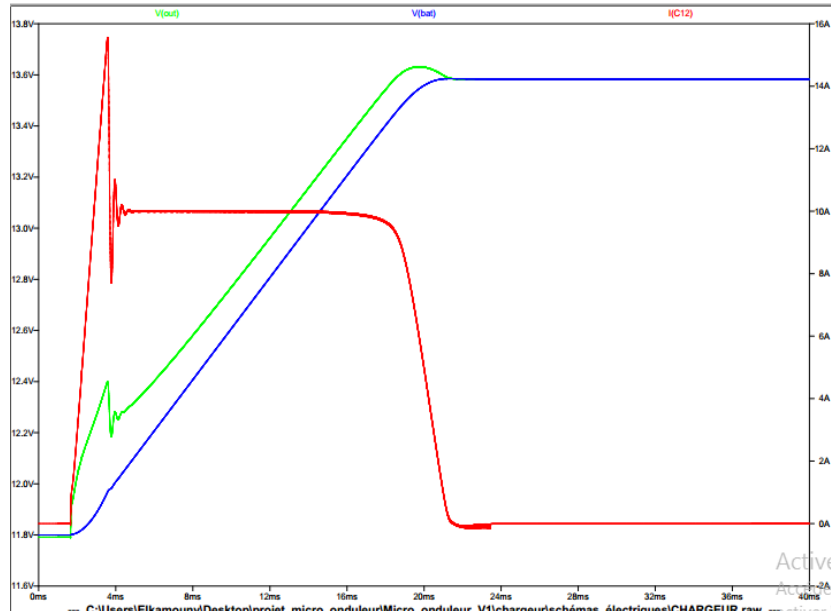

Fig. 8: charging a lead battery (simulation result on LTSpice)

The green curve: output voltage of the circuit (R_{load}) (V).

The red curve: charge current of the battery (A).

The blue curve: charge voltage of the battery (V).

The charge current is programmed at 10 A, the current and the charge voltage values are respectively set at 10 A and 13.5V. These input values have effectively been achieved during the simulation.

The current becomes negative around the 22th milliseconds; this is where the battery starts to supply the load.
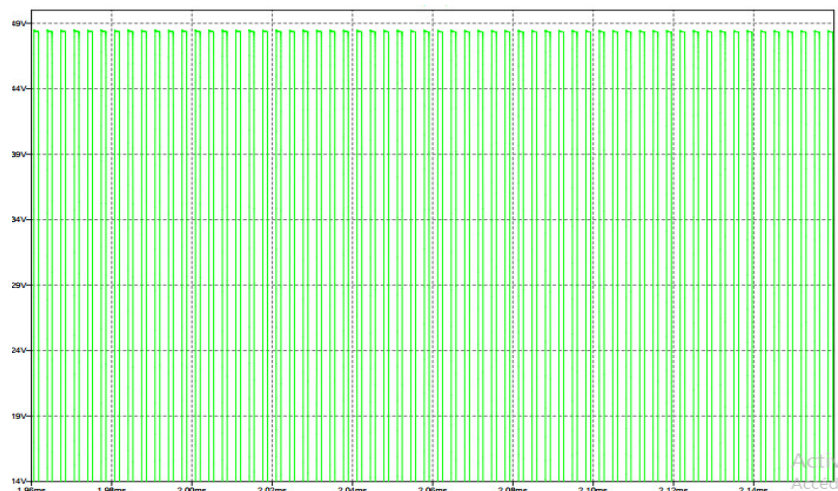

Fig. 9: The voltage in the Boost pin

The DC voltage of the photovoltaic panel is around 36V and the voltage value in the output of the boost is around 48V.
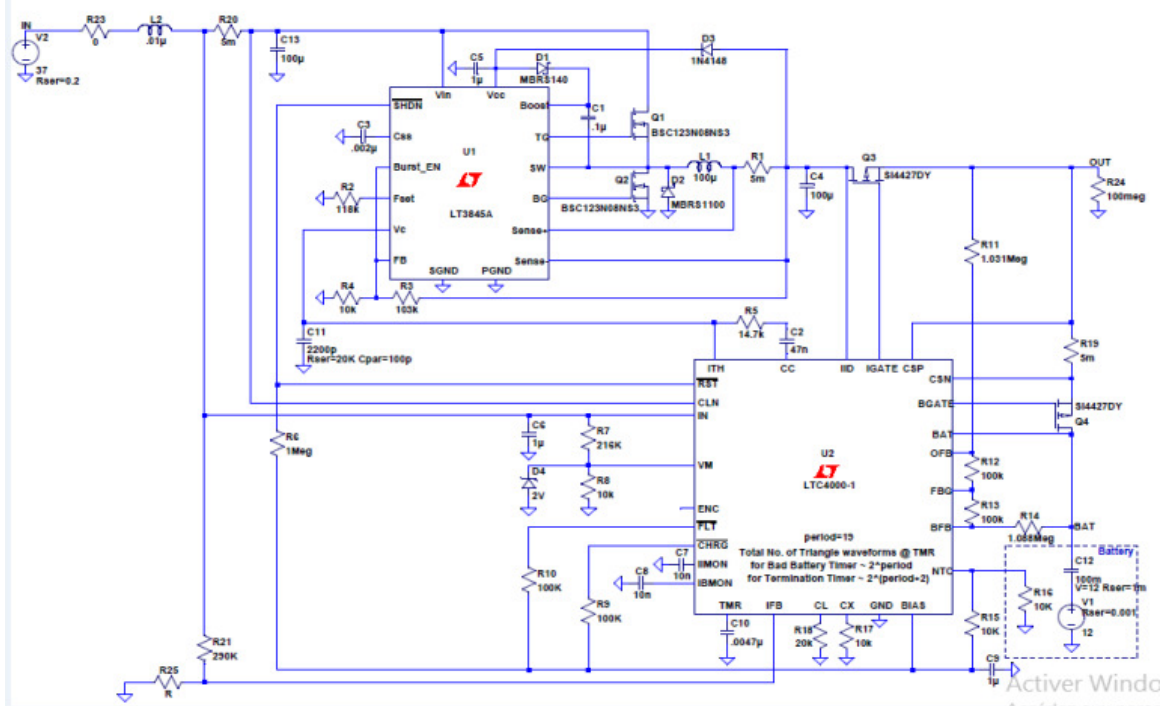

Fig. 10: Battery charger schematic

The schematic above is used to simulate the behaviour of the battery charger prototype on the LTSpice environment. In a first time, a voltage generator of 36V is used as a model of photovoltaic panel and the battery is modelled by a capacitor connected to a resistor. In second time, specific models for the battery and the photovoltaic panel are performed to show the different phases of the battery charging.

4. Conclusions

Several simulations and tests were made using a model of a lead acid battery of 12V. The charging process of this battery goes through an algorithm of three main phases are shown in Figure 7:
   - The transition phase (unstable) takes some milliseconds.
   - The constant current phase (I = 10A) it depends on the capacity of the battery.
   - The constant voltage phase: during this phase the battery keeps charging until the cancellation of the charge current.

For the practical test, A Sealed Lead Acid battery of 12V and 100Ah is used. To fortify the reliability and the safety of the battery charger, an intelligent system of control and management of the charging operation is provided.

For the validation of the proposed prototype, it is faced with many similar products in the market with results obtained through simulations and experimental measurements. The tests performed in MAScIR, the very rapid changes in environmental variables are considered. The results are satisfactory and ensure the feasibility of the solution.

References

[1] "*le monde des accumulateurs et des batteries rechargeables*" [Online]. Available: http:// *http://www.ni-cd.net/* 2014.

[2] "*LT3845A*" Datasheet, Document ref 3845afa, linear technology corporation 2010.

[3] J.Y LE CHENADEC "Alimentation à decoupage", ARMAND 173 Bd de strassbourg.

[4] (2014) Linear Technology "*LTC4000*-1". [Online]. Available: http:// *www.linear.com/*.

[5] "*LTC4000*-1" Datasheet Document ref 40001fa, linear technology corporation 2012.

[6] V.Boitier, C. Alonso "Dimensionnement d'un système photovoltaique" CETSIS'2005, Nancy, 25-27 octobre 2005.

[7] Jacques Bernard, " Energie Solaire", Coll. Génie Energétique, Ed. Ellipses, 2004.

[8] Anne Labouret, Michel Villoz, "Energie solaire photovoltaïque, manuel du professionnel", Ed. Dunod, 2003.

[9] Jin-Woo Jung and Ali Keyhani, "Control of a Fuel Cell Based Z-Source Converter", IEEE Transaction son Energy Conversion, Volume 22, No. 2, June 2007, pp. 467-476

[10] T. Markvart and L. Castaner, Practical Handbook of Photovoltaics, Fundamentals and Applications. Elsevier, 2003.

[11] Adel El Shahat, "Maximum Power Point Genetic Identification Function for Photovoltaic System", International Journal of Research and Reviews in Applied Sciences, June 2010.

[12] Mikkel C. W. Høyerby, Michael A.E. Anderssen, "Envelope Tracking Power Supply with fully controlled 4th order Output Filter", Applied Power Electronics Conference and Exposition, 2006. Twenty-First Annual IEEE, 19-23 March 2006.

[13] S. Lalouni, D. Rekioua, T. Rekioua, E. Matagne Fuzzy logic control of stand-alone photovoltaic system with battery storage ,Journal: of power sources, vol. 193, no. 2.

[14] D. Rekioua and E. Ernest, Optimization of Photovoltaic Power System: Modelization, Ed.Springer; (2012).

[15] A. El Jouni, R. El Bachtiri, & J.Boumhidi, Sliding mode control strategies for PV pumping System using boost converter, *Conference on Systems and Control (CSC'2007)* Mai, 16-18, Marrakech,Morocco, 2007.

[16] Emad M.Ahmed, Masahito Shoyama, Variable step size maximum power point tracker using a single variable for stand-alone battery storage PV systems, *Journal of Power Electronics, 11*(2), 218-227, 2011.